

Speaker membrane as Helmholtz resonator

Miłosz DERŻKO 🗅, Adam PILCH 🗅

AGH University of Krakow, al. Mickiewicza 30, Krakow, Poland

Corresponding author: Miłosz DERŻKO, email: milder@agh.edu.pl

Abstract In this study, we propose an innovative method for augmenting loudspeaker performance through the integration of a Helmholtz resonator into the speaker membrane. Conventional ported enclosures typically depend on a separate bass-reflex tube to enhance low-frequency efficiency. In contrast, our approach involves embedding the resonator within the membrane's structure. Various diaphragm configurations are analysed, including an empty reference membrane, a diaphragm with a simple aperture, and a diaphragm with an extended aperture (tube) to augment the inertial mass of the air. The interaction of the acoustic and structural domains is simulated utilizing COMSOL Multiphysics, and a Particle Swarm Optimization (PSO) technique is applied to refine the resonator geometry. The findings indicate that embedded apertures and tubes can effectively adjust resonance characteristics and enhance efficiency within targeted frequency bands, thereby introducing new avenues for the development of compact and high-performance loudspeaker enclosures.

Keywords: Helmholtz resonator, speaker membrane, electroacoustics, FEM, optimisation.

1. Introduction

Speakers are utilized in a wide range of applications, from compact devices such as smartphones to large-scale concert systems. Over the past decades, the fundamental understanding of loudspeakers has been grounded in the mechanical-acoustic-electrical analogy introduced by Beranek [1]. Building upon this foundation, Thiele and Small developed a set of parameters [2, 3] that provide a practical and theoretical Methodology for designing bass-reflex speaker enclosures. These parameters, known as Thiele-Small parameters, encompass key electrical and mechanical characteristics that define the performance and acoustic properties of loudspeaker systems.

The most prevalent types of speaker enclosures include sealed, ported, and band-pass designs. Among these, ported enclosures are widely employed for subwoofers and woofers due to their ability to enhance efficiency within specific frequency bands, particularly at low frequencies. A common feature of ported enclosures is the inclusion of a bass-reflex tube, which functions as an acoustic mass element in a Helmholtz resonator [4]. The geometry and placement of the bass-reflex tube are critical and must be optimized based on the desired tuning frequency of the enclosure. This study proposes an experimental approach to position the port as close as possible to the driver, thereby exploring its impact on the acoustic performance of the system.

2. Idea

Most woofers are designed with ported enclosures, which utilize an air cavity to create an acoustic resonance circuit. This port, referred to as a bass-reflex tube, is a common feature in loudspeaker enclosures. The resonance is caused by the moving mass of air in the tube, forming a Helmholtz resonator [5]. This configuration enhances the efficiency of the speaker within a specific frequency range. The placement of the tube is strictly correlated with the phase of the air pressure wave generated by the rear side of the loudspeaker diaphragm . The back surface of the membrane produces a sound wave with a different phase, necessitating the propagation path of the sound to be matched to a specific frequency band.

In the proposed design, the bass-reflex tube is integrated directly into the loudspeaker membrane. Fig. 1 illustrates the considered geometries, showcasing three membrane structures. Figs. 1b and 1c also depict the representation of the acoustic resonator components. The green block represents the acoustic inertia, which is placed on the red air spring. In the case of the diaphragm with a hole, the acoustic mass has a depth equal to the thickness of the membrane.

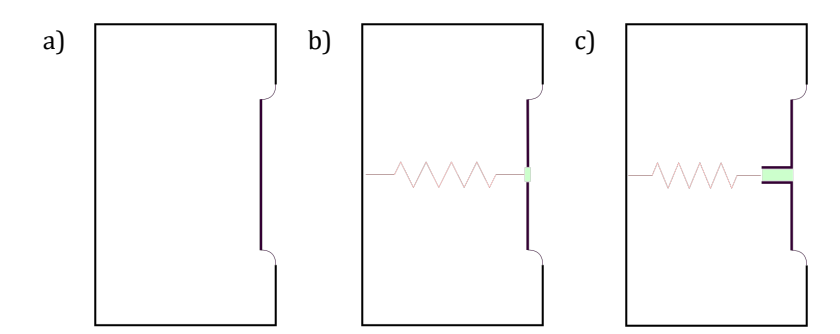


Figure 1. Comparison of the investigated membrane structures: a) empty membrane, b) membrane with hole, c) membrane with extended hole

A uniform force was applied to the rear surface of the membranes to ensure a consistent comparison across all structures. This approach isolates the influence of the membrane design by minimizing the impact of the closed enclosure, which typically acts as an additional spring, thereby increasing the stiffness of the mechanical system. By directly applying force to the membrane, the effects of the enclosure on the results are effectively eliminated.

3. Geometry

The system's geometry was modelled utilizing COMSOL Multiphysics software, specifically employing the Pressure Acoustics and Solid Mechanics modules. The model comprises three principal components: the air volume (green), wherein acoustic waves propagate; the membrane (grey), which is suspended within the enclosure; and the rigid walls and loudspeaker enclosure (brown), which account for thermo-acoustic phenomena. These components are illustrated in Fig. 2a.

To optimize computational efficiency, the geometry was reduced to a quarter section with mirror boundary conditions applied. A four-neck Helmholtz resonator was integrated with the membrane to achieve resonance at low frequencies, as documented in [6, 7]. The air volume was modelled with a radius of 50 cm to mitigate near-field wave effects. A Perfectly Matched Layer (PML) was implemented at the boundaries of the air volume to absorb outgoing waves and prevent reflections. Additionally, a 3 cm-thick Exterior Field Calculation layer was included near the centre to facilitate directivity analysis. The enclosure was conceptualized as a rigid, non-vibrating structure incorporated within an infinite baffle to emulate realistic boundary conditions. The membrane, with a diameter of 5 cm, was suspended inside the enclosure. The comprehensive geometry is illustrated in Fig. 2a, with a detailed view of the basic membrane provided in Fig. 2b. The evaluated diaphragm configurations are presented in Figs. 3a, 3b, and 3c.

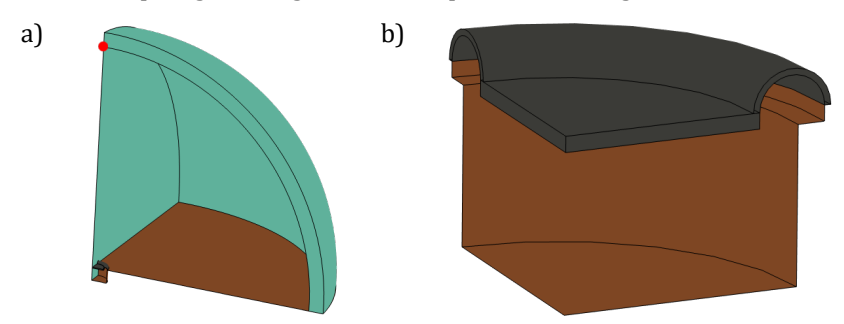


Figure 2. Visualization of the membrane geometries in COMSOL: a) general model geometry, b) closer view of the empty membrane.

All cross-sectional views include a dashed line representing the symmetry boundary. A comparative analysis of the configurations will be conducted based on the sound pressure level characteristics. The measurement point is in front of the membranes, within the exterior field layer. The position of the probe is marked by a red sphere in Fig. 2a.

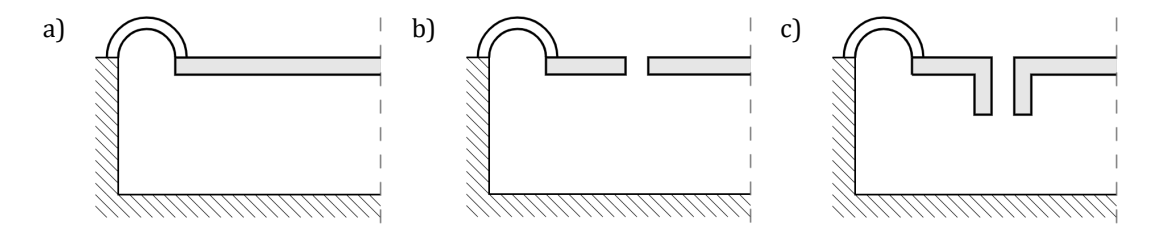


Figure 3. Cross-sections of all investigated geometry structures: a) empty membrane, b) membrane with hole, c) Membrane with extended hole.

4. Helmholtz resonator

To ensure a consistent comparison across the considered cases, it is essential to establish a standardized method for quantifying the dimensions of the loudspeaker enclosure and neck corresponding to a specified resonant frequency. The resonant frequency of a Helmholtz resonator can be expressed as:

$$f_{\rm res} = \frac{c}{2\pi} \sqrt{\frac{A}{V L_{\rm eff}}},\tag{1}$$

where c represents the speed of sound in air, A denotes the cross-sectional area of the neck, V is the volume of the cavity, and $L_{\rm eff}$ is the effective length of the neck, accounting for end corrections. Numerous parameters influence the resonant frequency, making it challenging to determine the appropriate dimensions for a specific frequency.

To address this challenge, an optimization algorithm was employed to identify the optimal dimensions of the resonator. The Particle Swarm Optimization (PSO) algorithm was selected for this purpose. PSO is a population-based optimization technique inspired by the social behaviour of birds and fish. It has proven effective in solving complex optimization problems across various domains, including acoustics [8, 9]. Further details on this technique can be found in the MATLAB documentation [10]. The PSO algorithm requires multiple iterations of calculations, which can be computationally expensive, particularly for models incorporating membrane geometry.

To reduce computational complexity and focus the investigation on key phenomena, a simplified model of the Helmholtz resonator was developed, omitting the *Structure Integration* node and considering only the frequency domain.

The cost function for the optimization process is based on the sound absorption coefficient α , which quantifies the ratio of absorbed to incident sound energy at a given frequency. A peak in the α curve indicates the resonator's operational frequency range, signifying its influence on the loudspeaker enclosure. The cost function is defined as the mean square error between the target and the calculated α curve, enabling the PSO algorithm to minimize this error and optimize the resonator's performance.

4.1. Numerical model

To evaluate the sound absorption coefficient curve, a numerical model was developed. As described in Sect. 2, two primary enclosure configurations were investigated: one with a hole and another with a tube. These configurations were incorporated into the resonator model. Fig. 4 illustrates the geometries of the two investigated models, along with the parameters used in Eq. 1.

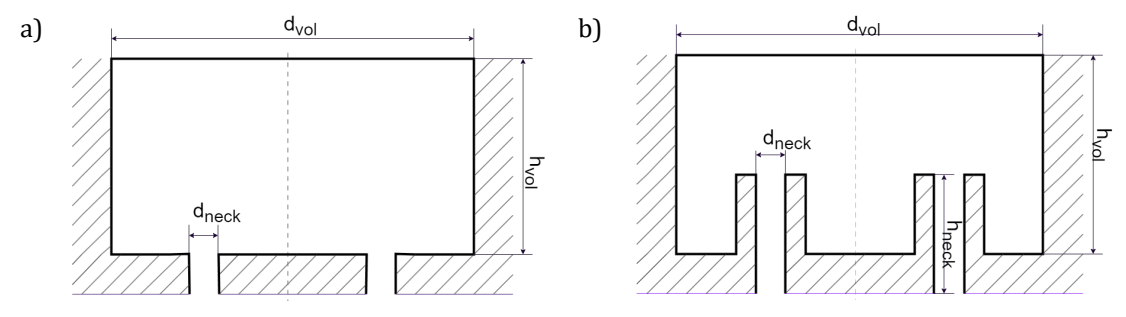


Figure 4. Geometries of the investigated Helmholtz resonator configurations:

a) Optimized dimensions of the resonator with a holes, b) Optimized dimensions of the resonator with a tubes.

The sound absorption coefficient was determined by calculating the ratio between the incident and reflected pressure. To achieve this, all resonators were analysed within a tube using the *Background Pressure Field* [11] node, which generates an incident plane wave.

The pressure wave at certain locations was assessed at specified points marked on red sphere on Fig. 2a. Fig. 5a illustrates the model along with the chosen measurement plane, while Fig. 5b displays the computed α curve for a sample resonator. This model was utilized to verify the method for determining the sound absorption coefficient. The resonator underwent analysis across a frequency spectrum from 63 Hz to 5 kHz. The resonator's dimensions can be found in Tab. 1.

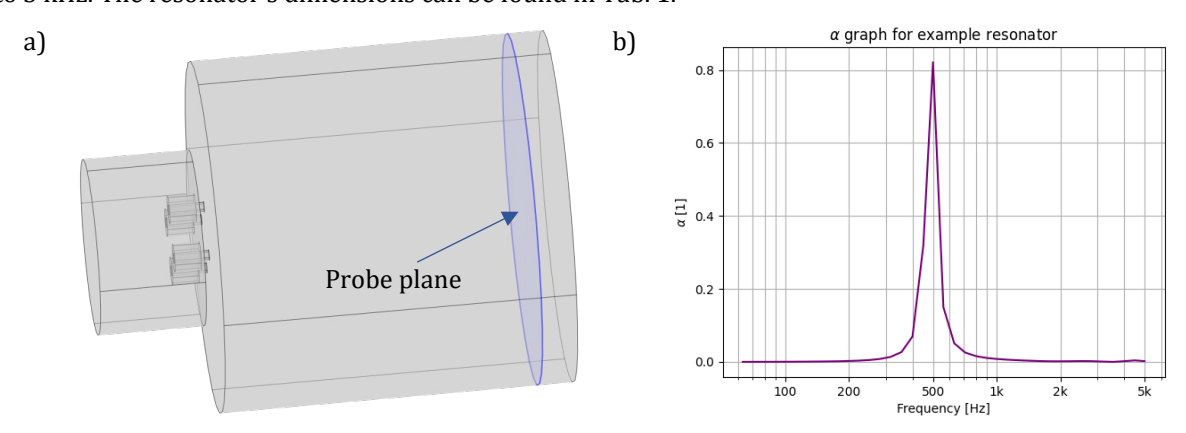


Figure 5. Visualization of analysed Helmholtz resonator model and α result: a) Helmholtz resonator model with the selected probe plane, b) Sound absorption coefficient for an example resonator.

Table 1. Dimensions of analysed Helmholtz resonator model.

Parameter	Value [mm]	
Neck diameter (d_{neck})	3	
Neck height (h_{neck})	10	
Cavity diameter (d_{vol})	50	
Cavity height (h_{vol})	30	

Using Eq. 1, the calculated resonance frequency was approximately 450 Hz, which aligns closely with the α curve shown in Fig. 5b. The divergences between them may be due to the use a four-neck resonator instead of one neck. This model is now prepared for optimization to identify the best combination of parameters for the desired frequencies. However, before proceeding, the cost function must be defined.

4.2. Cost function

The sound absorption coefficient of a Helmholtz resonator exhibits a resonant behaviour [12]. To facilitate optimization, a reference function was defined. Ideally, this function would take a value of one within the resonant frequency range and zero elsewhere. However, such a definition poses challenges for the optimizer in identifying the appropriate direction to adjust the resonance [13]. To address this, a homographic function was employed instead of zeros, ensuring smoother transitions and improved optimization performance. The reference α curve is defined as follows:

$$\alpha_{ref} = \begin{cases} 1 & \text{for } f \in (f_{res} - \Delta f, f_{res} + \Delta f) \\ \frac{\Delta f}{f - f_{res}} & \text{for } f \notin (f_{res} - \Delta f, f_{res} + \Delta f) \end{cases}$$
 (2)

where $f_{\rm res}$ represents the target resonance frequency of the structure, and Δf denotes the assumed bandwidth of the resonator's operational frequency range. Fig. 6 illustrates example reference α curves for different values of Δf with $f_{\rm res} = 500$ Hz.

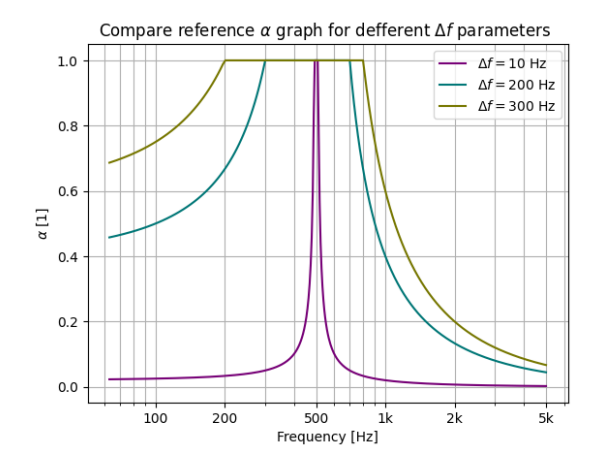


Figure 6. Example reference sound absorption coefficient curves for different Δf values with $f_{\rm res} = 500$ Hz.

The maximum values of α_{ref} are concentrated around the target frequency, effectively replicating the resonator's behavior. The cost function for the optimization process is subsequently defined as the root mean square error (RMSE) between the calculated α and the reference α_{ref} curves. The cost function can be defined by the following equation:

$$J = \sqrt{\frac{1}{N} \sum_{i=1}^{N} (\alpha(i) - \alpha_{ref}(i))^2},$$
(3)

where *N* represents the number of frequency points considered. The PSO algorithm minimizes *J* to determine the optimal geometrical dimensions of the resonator.

4.3. Optimization result

The optimization process was conducted for three target frequencies: 300 Hz, 400 Hz, and 500 Hz, for each of the two geometrical configurations. The PSO algorithm was configured with a population size of 10 particles and a maximum of 100 iterations. Under these settings, the optimization process required approximately four hours to complete.

The parameter ranges for the optimization were determined based on the physical constraints of the resonator design and are summarized in Tab. 2. The results of the optimization, including the optimized parameters and the corresponding cost function values, are presented in Tabs. 3 and 4.

Table 2. Parameter ranges for optimization.

Parameter	Min [mm]	Max [mm]
d_{neck}	0.5	15
h_{neck}	1	10
d_{vol}	60	200
h_{vol}	20	60

Table 3. Optimization results for membrane with tube.

Parameter	Target f_{opt}			
raiailletei	300 Hz	400 Hz	500 Hz	
d_{neck}	5.46	7.07	9.81	
h_{neck}	3.78	6.82	9.53	
d_{vol}	65.77	60.09	60.00	
h_{vol}	26.70	21.59	20.00	

Table 4. Optimization results for membrane with hole.

Parameter	Target f_{opt}			
raiailletei	300 Hz	400 Hz	500 Hz	
d_{neck}	4.49	5.21	8.88	
d_{vol}	60.01	60.00	64.73	
h_{vol}	31.70	20.00	24.26	

The results demonstrate that the optimization successfully identified parameter sets that minimize the cost function for each target frequency. The optimized geometries can now be implemented in the resonator design to achieve the desired acoustic performance.

5. Applying to enclosure

The membranes were designed and implemented based on the dimensions provided in Tabs. 3 and 4. The corresponding sound pressure level (SPL) results for the optimized configurations are presented in Fig. 7. These results compare the acoustic performance of membranes with two distinct geometries: one employing tube and the other employing holes.

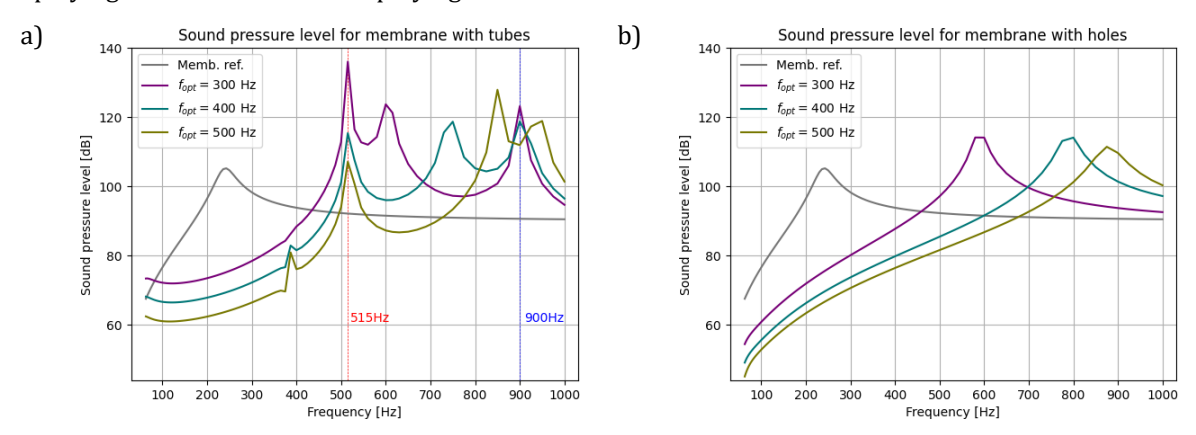


Figure 7. Comparison of sound pressure levels for membranes with: a) tubes, b) holes.

The tube-based configuration exhibits two distinct types of resonances. The first type consists of tuneable resonances that align with the targeted optimization frequencies, like those observed in the membrane with holes. The second type comprises invariant resonances that remain stable across all optimized cases. Specifically, two dominant fixed-frequency resonances are identified: one at approximately 515 Hz (indicated by the red dashed line) and another near 900 Hz (blue dashed line). These elevated SPL values are attributed to structural vibrations of the attached tubes rather than to the acoustic response of the membrane itself. The observed SPL peaks may also result from the absence of air suspension in the model.

To accurately identify the resonance frequency of the Helmholtz resonator, excluding membrane modes, the particle velocity distribution was analysed. At the resonance frequency of the Helmholtz resonator, an increase in particle velocity at the neck is observed, as shown in Fig. 8b. To simplify the detection of resonance frequencies, the average particle velocity across all frequencies was analysed (Fig. 8a).

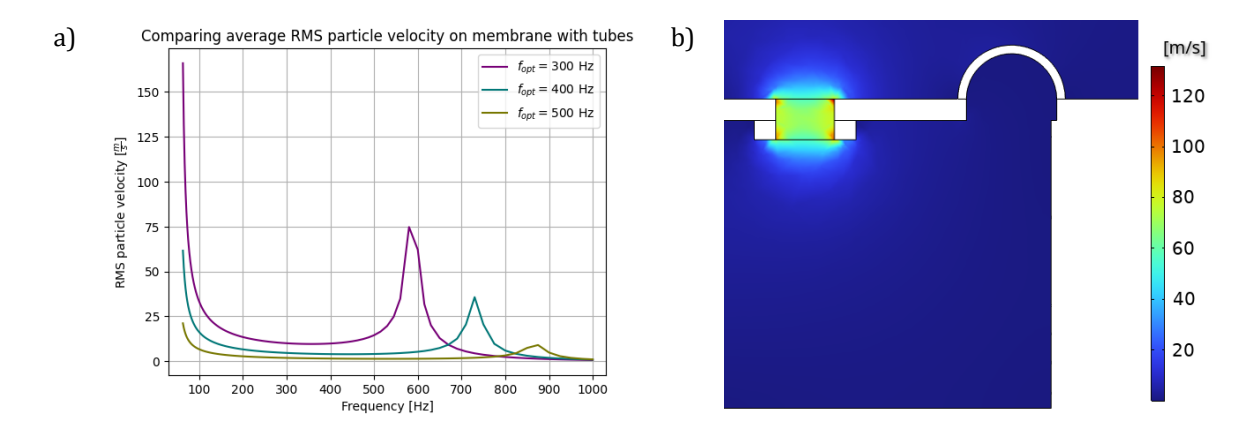


Figure 8. Analysis of particle velocity characteristics for the membrane with tubes: a) frequency-dependent average RMS particle velocity magnitude for the membrane with tubes, b) spatial distribution of particle velocity at 580 Hz for the target frequency $f_{opt} = 300$ Hz.

The calculated and optimized resonance frequencies for each configuration are summarized in Tab. 5, which provides both the calculated resonance frequencies and the corresponding tested Helmholtz resonator frequencies for each geometry. The calculations for the holes and tubes were conducted by determining the maximum SPL values, whereas the maximum reference Helmholtz resonator value was ascertained via the alpha parameter. All calculations were executed with a resolution of 3.5 Hz.

Table 5. Matrix of optimized and calculated frequencies for different configurations.

Coometry	Target f_{opt}		
Geometry	300 Hz	400 Hz	500 Hz
Reference Helmholtz resonator	311.2	401.0	499.0
Holes	592.4	783.3	917.2
Tubes	588.9	730.3	868.2

Notably, the observed resonances occur at frequencies approximately twice as high as the optimized values. This frequency discrepancy is likely attributable to deviations from the ideal Helmholtz resonator model, including imperfect coupling with the enclosure, leakage effects, or variations in effective acoustic compliance.

The results presented in this study demonstrate a significant enhancement in acoustic performance for both modified configurations. Specifically, the sound pressure level increases by approximately 20 dB relative to the unmodified membrane. However, this improvement is confined to narrow frequency bands around the optimized resonance frequencies, underscoring the strong spectral selectivity and localized efficiency of the acoustic response. These findings highlight the potential of structural modifications in tailoring the dynamic behaviour of membranes for specific acoustic applications.

6. Conclusion

This study explored the impact of structural modifications, specifically tubes and holes, on the acoustic performance of loudspeaker membranes. The comparative analysis of the two configurations reveals distinct advantages and limitations. The perforated membrane design demonstrates a simpler implementation with substantial improvements in sound pressure level (SPL), making it a viable option for cost-effective manufacturing. Conversely, the tube-based configuration introduces additional resonance modes, offering greater flexibility in tuning but at the expense of increased complexity and potential mechanical resonances.

Future work will focus on addressing these challenges by refining the acoustic models to better predict the behaviour of tube-induced resonances. Additionally, empirical validation through prototype fabrication and experimental measurements will be conducted to confirm the numerical findings. Further investigations will also explore the integration of electrical models to provide a holistic understanding of the loudspeaker system's performance. These efforts aim to optimize the structural modifications and establish a comprehensive framework for designing high-efficiency loudspeaker membranes tailored to specific acoustic applications, such as compact subwoofers for consumer audio systems.

Acknowledgments

This work was partly supported by a research subsidy of the Faculty of Mechanical Engineering and Robotics, AGH University of Krakow, no. 16.16.130.942.

Additional information

The authors declare: no competing financial interests and that all material taken from other sources (including their own published works) is clearly cited and that appropriate permits are obtained.

References

- L.L. Beranek; Acoustics; Acoustics Laboratory, Massachusetts Institute of Technology, Cambridge, 1954
- 2. A.N. Thiele; Loudspeakers in Vented Boxes. Part I; Australian Broadcasting Commission, 2001
- 3. A.N. Thiele; Loudspeakers in Vented Boxes. Part II; Australian Broadcasting Commission, 2001
- 4. A. Bezzola; Optimal Bass Reflex Loudspeaker Port Design; In: Proceedings of the COMSOL Conference, Boston, USA, 2019
- 5. N. Deshler; The Helmholtz Resonator; Bachelor's Thesis, Physics Department, University of California, 2021
- 6. N.M. Papadakis, G.E. Stavroulakis; Tunable Helmholtz Resonators Using Multiple Necks; Micromachines, 2023, 14, 1–14; DOI: 10.3390/mi14101932
- 7. N.M. Papadakis, G.E. Stavroulakis; FEM Investigation of a Multi-Neck Helmholtz Resonator; Applied Sciences, 2023, 13, 1–16; DOI: 10.3390/app131910610
- 8. R. Barbieri, N. Barbieri, K.F. de Lima; Some Applications of the PSO for Optimization of Acoustic Filters; Applied Acoustics, 2015, 89, 62–70; DOI: 10.1016/j.apacoust.2014.09.007
- 9. A.M. Shaaban, C. Anitescu, E. Atroshchenko, T. Rabczuk; Isogeometric Boundary Element Analysis and Shape Optimization by PSO for 3D Axi-Symmetric High Frequency Helmholtz Acoustic Problems; Journal of Sound and Vibration, 2020, 486, 1–30; DOI: 10.1016/j.jsv.2020.115598
- 10. MathWorks; Particle Swarm Optimization Algorithm; https://www.mathworks.com/help/gads/particle-swarm-optimization-algorithm.html (accessed on 2025.04.29)
- 11. COMSOL; Acoustics Module User's Guide; https://doc.comsol.com/5.4/doc/com.comsol.help.aco/AcousticsModuleUsersGuide.pdf (accessed on 2025.04.29)
- 12. F. Langfeldt, H. Hoppen, W. Gleine; Resonance Frequencies and Sound Absorption of Helmholtz Resonators with Multiple Necks; Applied Acoustics, 2019, 146, 314–319; DOI: 10.1016/j.apacoust.2018.10.021
- 13. J. Kennedy, R. Eberhart; Particle Swarm Optimization; In: Proceedings of ICNN'95 International Conference on Neural Networks; IEEE, 1995, 1942–1948; DOI: 10.1109/ICNN.1995.488968

© **2025 by the Authors.** Licensee Poznan University of Technology (Poznan, Poland). This article is an open access article distributed under the terms and conditions of the Creative Commons Attribution (CC BY) license (http://creativecommons.org/licenses/by/4.0/).